Enhanced superconductivity at the interface of W/Sr_2RuO_4 point contacts

He Wang (王贺), Weijian Lou (娄伟坚), Jiawei Luo (骆佳伟), and Jian Wei (危健)*
International Center for Quantum Materials, School of Physics, Peking University, Beijing 100871, China
and Collaborative Innovation Center of Quantum Matter, Beijing, China

Y. Liu
Department of Physics and Materials Research Institute, The Pennsylvania State University, University Park, Pennsylvania 16802, USA
and Department of Physics and Astronomy and Key Laboratory of Artificial Structures and Quantum Control (Ministry of Education), Shanghai Jiao Tong University, Shanghai 200240, China

J. E. Ortmann and Z. Q. Mao
Department of Physics, Tulane University, New Orleans, Louisiana 70118, USA
(Received 6 January 2015; revised manuscript received 6 April 2015; published 22 May 2015)

Differential resistance measurements are conducted for point contacts (PCs) between the Sr_2RuO_4 (SRO) single crystal and the tungsten tip approaching along the *c* axis direction of the crystal. Since the contact is made at liquid helium temperature and the tungsten tip is hard enough to penetrate through the surface layer, consistent superconducting features are observed. First, with the tip pushed towards the crystal, the zero-bias conductance peak (ZBCP) due to Andreev reflection at the normal-superconducting interface increases from 3% to more than 20%, much larger than previously reported, and extends to temperatures higher than the bulk transition temperature. Reproducible ZBCP within 0.2 mV may also help determine the gap value of SRO, on which no consensus has been reached. Second, the logarithmic background can be fitted with the Altshuler-Aronov theory of electron-electron interaction for tunneling into quasi-two-dimensional electron systems. Feasibility of such fitting confirms that spectroscopic information such as density of states is probed, and electronic temperature retrieved from such fitting can be important to analyze the PC spectra. Third, at bias much higher than 0.2 mV there are conductance dips due to the critical current effect. These dips persist up to 6.2 K, possibly due to enhanced superconductivity under uniaxial pressure.

DOI: 10.1103/PhysRevB.91.184514 PACS number(s): 74.70.Pq, 74.45.+c, 74.62.Fj, 74.62.En

I. INTRODUCTION

The layered perovskite ruthenate Sr_2RuO_4 (SRO) has shown evidence for spin-triplet, odd-parity superconductivity (SC) which may be useful for topological quantum computation [1–3]. The possible chiral orbital order parameter for the two-dimensional SC is $p_x \pm ip_y$ as suggested by the time-reversal symmetry breaking experiments [4,5]. Such chiral order is expected to generate edge currents, but the expected magnetic field due to edge currents has not been directly observed with local field imaging [6–8], though there is indirect evidence of edge currents revealed by in-plane tunneling spectroscopy [9,10] and point contact spectroscopy (PCS) [11,12], both requiring assumptions to fit the conductance spectra, and the fitting parameters including the gap value are not consistent with each other.

The surface properties of SRO are a critical factor for field imaging with scanning quantum interference devices, as well as for the tunneling and point contact spectroscopy. It is known that the SRO surface can undergo reconstruction and the intrinsic SC may not be probed [13,14], and it may even show ferromagnetism (FM) due to lattice distortion [15]. Very careful *in situ* preparation of devices is required for making good tunnel junctions using microfabrication techniques [9]. Recently there is also a theoretical proposal that surface disorder indeed can destroy the spontaneous currents [16].

One way to overcome the surface layer problem is to use a hard tip for the point contact (PC) measurement. If the tip is hard enough, it may penetrate through the surface dead layer and probe the SC underneath [17]. In fact, for this reason tungsten tips have been used for PCS of heavy-fermion superconductors [18]. A consequence of using a hard tip is that the tip will exert some pressure on the surface which may affect the SC [19], possibly due to local distortion of the lattice [20,21]. It is known that for SRO a very low uniaxial pressure of 0.2 GPa along the *c* axis can enhance the superconducting transition temperature (T_c) of pure SRO from 1.5 K up to 3.2 K [22,23], and recently in-plane strain (0.23%) along the ⟨100⟩ direction has also been shown to enhance T_c from 1.3 K up to 1.9 K [24]. The pressure in the above-mentioned measurements was applied to the whole crystal sample, while for PCs the pressure is exerted locally on a small region of the sample. In the latter case it may be less affected by the inhomogeneity of the applied pressure and the sample tends less to developing cracks; thus locally higher pressure may be reached although the absolute pressure is not known. Here we report greatly enhanced SC observed at the interface of the point contact junction between SRO single crystals and the tungsten tip approaching along the *c* axis direction.

II. METHODS

SRO single crystals are grown by the floating zone methods and are from two different batches; details of sample

*weijian6791@pku.edu.cn

preparation can be found in previous reports [25]. The bulk T_c is about 1.5 K by standard resistance measurement. Sample S1 is from the first batch and is easier to cleave and shows no Ru inclusions. Sample S2 is from the second batch, difficult to cleave, and contains many Ru inclusions [for optical images of the surface and $R(T)$ of the bulk samples, see Appendix C]. Only on the freshly cleaved surface of S1 do we observe clear features of SC. Tungsten wire of 0.25 mm diameter is etched to form the tip. The silicon chip with the sample and thermometer glued on top is mounted on an attoCube nanopositioner stack. Since the tip and sample are both fixed to the copper housing, relative displacement between the tip and sample is suppressed, which ensures a stable contact and reproducible PC spectra. The housing is suspended with springs at the bottom of a insertable probe for a Leiden dilution fridge. With such customization, the sample position is not at the field center of the magnet, but the field value can be estimated with the tabled values from the magnet manufacturer. Differential resistance (dV/dI) is measured with standard lock-in technique, and for easy comparison with theory, the reciprocal of dV/dI is plotted, which is close to dI/dV when the excitation is small.

III. RESULTS AND DISCUSSIONS

At the same location, by pushing the tungsten tip towards the SRO surface (technically it is the SRO sample moving towards the tip), the PC resistance is reduced and the pressure is increased (see Appendix D for reproducibility and data acquired in other runs; see Appendix A for the model of PC resistance). The zero-bias and zero-field resistance (R_0) is 9.3, 4.3, 3.2 Ω, respectively, and the bias dependence of dI/dV is shown in Figs. 1(a), 1(c), and 1(e), at the nominal temperature 0.35 K. SC is clearly shown by the zero-bias conductance peak (ZBCP), a domelike feature within ±0.2 mV at zero applied field. With a 625 Oe magnetic field applied along the c axis ($H_\perp$), SC is almost fully suppressed for the 9.3 Ω PC as shown by the conductance dip at zero bias. However, for the 4.3 Ω PC, there is still a small conductance dome at 625 Oe, suggesting that SC is not fully suppressed; i.e., SC is enhanced with increased pressure.

Enhancement of SC is further confirmed by the temperature dependence of dI/dV at zero field as shown in Fig. 2(b) and Fig. 3(b), where T_c is increased from the bulk value of 1.5 K to about 2 K and 2.5 K for the 9.3 Ω and 4.3 Ω PCs, respectively. This enhancement of SC is consistent with previous susceptibility measurements on bulk SRO samples under uniaxial pressure, where the mechanism of T_c enhancement was ascribed to anisotropic lattice distortion [22,23,26], similarly to that found in the eutectic 3 K phase [27,28].

A. Magnetoresistance

The magnetoresistance (MR) is shown in Figs. 1(b), 1(d), and 1(f) for the three PCs [for consistency with Figs. 1(a), 1(c), and 1(e), conductance is plotted, but MR is still used in description]. The conductance starts to decrease quickly at around 400 Oe, and there is clearly a hysteresis with jumps which get sharper and more pronounced for higher PC pressure (lower PC resistance). MR hysteresis is usually observed for

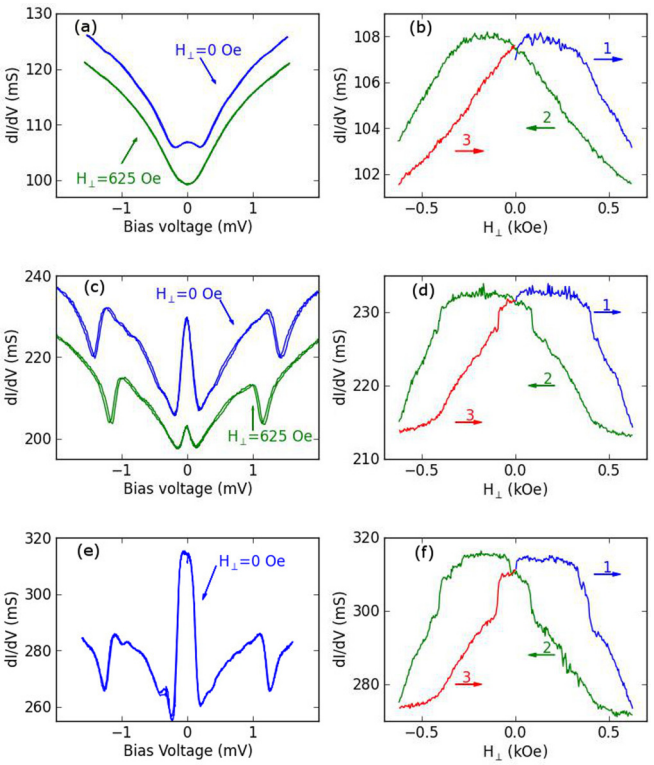

FIG. 1. (Color online) Bias dependence of dI/dV [(a), (c), (e)] and magnetoresistance [(b), (d), (f)] of three point contacts (PCs) formed at the same location between the W tip and SRO single crystal S1 at 0.35 K. The resistance at zero bias and zero field (R_0) is 9.3, 4.3, 3.2 Ω, respectively. For clarity, in (a) and (c) the dI/dV curves at 625 Oe (green) are shifted up by 2 and 10 ms, respectively. Arrows in (b), (d), (f) show the sweeping direction of the magnetic field. The reproducibility of the measurements is demonstrated by the overlapping of dI/dV curves in (a), (c), (e) with bias ramping in both directions. The discontinuity around ±625 Oe is related to the ramping speed of the field, and can be minimized when the field ramping speed is reduced, while the hysteresis is the same.

ferromagnetic samples, and the observation of both features of SC and MR hysteresis can be linked to the coexistence of SC and ferromagnetism (FM), e.g., for SC at the interface of oxides [29]. The question is whether the FM-like behavior can be related to the time-reversal symmetry breaking field [6–8].

First the simple origin of vortex pinning needs to be considered. The field value above which dI/dV starts to decrease quickly is around 400 Oe, which is of the same order of magnitude as the upper critical field $H_{c2}||c$ about 710 Oe for pure SRO crystal, but larger than the critical field $H_{c1}||c$ about 70 Oe (by specific-heat measurements) [30]. Increase of resistance at around 400 Oe could be due to vortices entering the PC region and the SC fraction being reduced [21], which would require a much enhanced H_{c1}. Although strongly enhanced H_{c1} by PCs has not been reported, enhancement of H_{c2} due to pressure for a Nb tip was previously found [21]. For a homogeneous vortex lattice the average distance between vortices is $\sim\sqrt{\Phi_0/H}$, about 0.3 μm at 400 Oe. Thus to include multiple vortices the diameter of the PC should be larger than 0.3 μm. The estimation of the PC diameter with the conventional model of the PC is tens of nanometers for

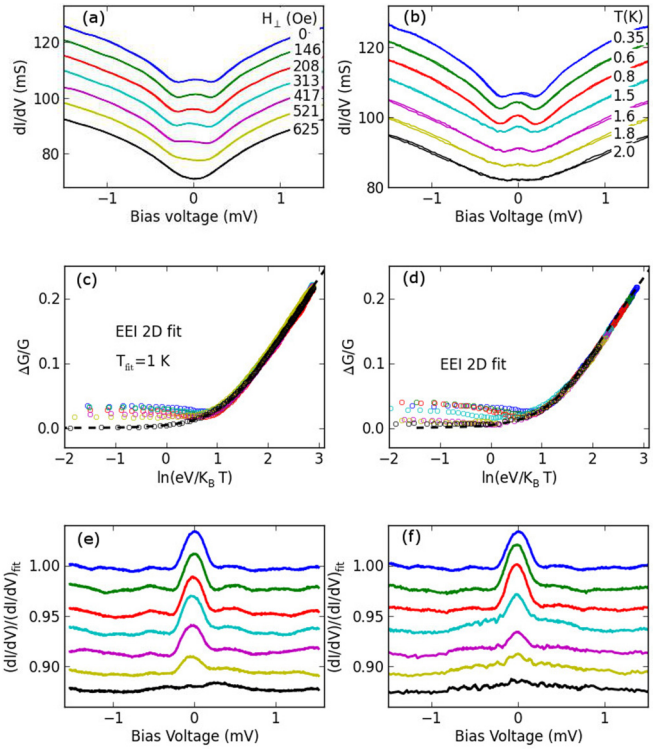

FIG. 2. (Color online) (a) Bias dependence of dI/dV for the 9.3 Ω point contact at 0.35 K with increasing $H_\perp$ and (b) zero-field dI/dV with increasing T. Curves are shifted for clarity except for the zero-field 0.35 K curve. (c) Fitting with EEI theory in the 2D limit for data in (a) with fitting temperature $T_{\rm fit} = 1.0$ K. (d) Fitting for data in (b) with $T = 0.35$ (1.0), 0.6 (1.1), 0.8 (1.24), 1.5 (1.65), 1.6 (1.85), 1.8 (1.95), and 2.0 (2.2) K from top to bottom ($T_{\rm fit}$ is indicated in the parentheses). After being normalized by the EEI fits with corresponding $T_{\rm fit}$, the curves are shown in (e) for different $H_\perp$ and (f) for different T. Curves in (a), (b), (e), and (f) are shifted for clarity.

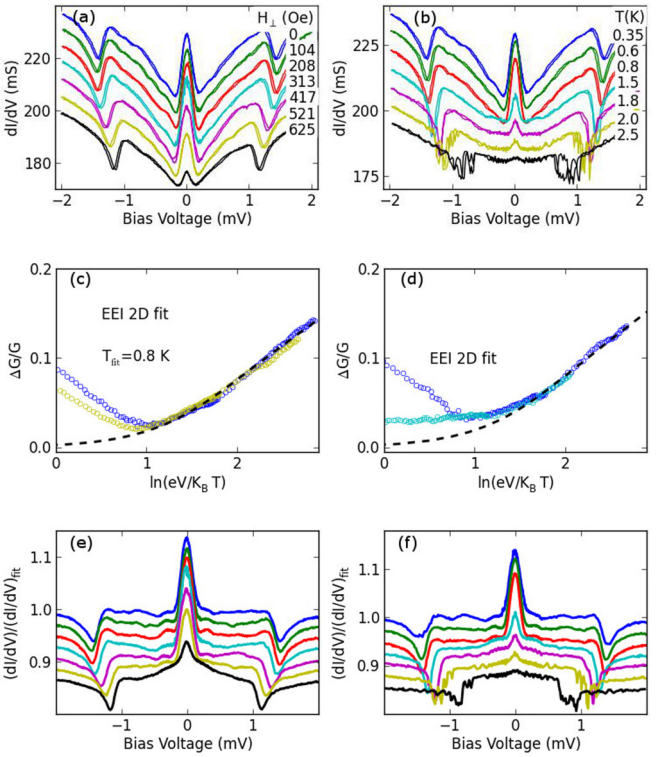

FIG. 3. (Color online) (a) Bias dependence of dI/dV for the 4.3 Ω point contact at 0.35 K and with increasing $H_\perp$ and (b) zero-field dI/dV with increasing T. Curves are shifted for clarity except for the zero-field 0.35 K curve. (c) Fitting with EEI theory in the 2D limit for $H_\perp = 0$ (blue) and 625 Oe (yellow) curves in (a) with $T_{\rm fit} = 0.8$ K, and (d) fitting for curves in (b) with $T = 0.35$ (0.8), 1.5 (1.5) K ($T_{\rm fit}$ is indicated in the parentheses). After being normalized by the EEI fits with corresponding $T_{\rm fit}$, the data curves are shown in (e) for different $H_\perp$ and (f) for different T. Curves are shifted for clarity.

PC resistance about 10 Ω, but if the model of distributed smaller PC junctions [21,31] is considered, then the area of the footprint can be much larger than the actual contact area within the footprint. Possibly related, a vortex droplet formed within a confined superconductor region can show discrete jumps of magnetization, which is associated with metastable vortex droplet and fission of vortices [32]. However, there is still some subtle difference; e.g., here for one ramping direction the MR jumps were found on both sides regarding zero field, but in the droplet case the magnetization jumps only appear on one side. We also note that such large hysteresis was not observed previously in PC measurements, so although vortex pinning seems to be possible, it still needs to be confirmed.

Besides conventional pinning, intrinsic pinning due to the chiral domain wall for SRO has been previously investigated [33], but it seems unlikely to reach 400 Oe. Note that hysteresis for threshold current was found by Kambara *et al.* [34] in narrowed eutectic SRO bridges with Ru lamellae, where the assumption is that there is a domain wall (DW) between antiparallel domains with chiral supercurrent flowing in opposite directions. DW motion induced by dc current is proposed to be the origin of the hysteresis in the bias dependence of dI/dV measurements, but here we do not find hysteresis in the bias dependence of dI/dV measurements. Thus intrinsic pinning does not seem to be the origin.

Hysteretic vortex pinning has been reported for superconductor-ferromagnet nanocomposites (Nb matrix with Gd particles) [35]. Surface FM on SRO was indeed predicted due to lattice distortion of surface reconstruction [15], but was not experimentally confirmed. Among layered perovskite ruthenates in the series $A_{n+1}Ru_nO_{3n+1}$, $SrRuO_3$ is a ferromagnetic metal with $T_c = 160$ K, and $Sr_3Ru_2O_7$ is at the border of FM and shows pressure-induced FM [36]. Thus it is not unexpected that FM could be induced for SRO, or there might be some eutectic phase [25] on the surface which leads to FM. Previously, experimental attempts to measure the magnetic susceptibility of bulk SRO with uniaxial pressure were unsuccessful, since above 0.4 GPa the SRO sample tends to crush [37], while no drastic change of the temperature dependence of susceptibility was observed. On the other hand, doping the Sr with Ca does show a ground state of *static* magnetic order due to rotation of RuO_6 octahedra [38,39]. If the pressure under the tip is higher than 0.4 GPa [17] then the effect may be comparable with that by doping. In fact FM alone may lead to MR hysteresis in point contact measurements due to the surface spin valve effect [40], but here the hysteresis

diminishes together with SC with increasing temperature (see Appendix E for the data), so there is still no clear evidence of surface FM.

B. Conductance enhancement near zero bias and the background

Except for the MR hysteresis, both field and temperature dependencies of dI/dV are similar to those found for in-plane Au/SRO tunneling junctions in Ref. [9], as shown in Fig. 2 and Fig. 3, for the 9.3 and 4.3 Ω PCs, respectively. We note that in Ref. [9] gap values 0.7 mV, 0.93 mV (active), and 0.28 mV (passive) have been used to fit the in-plane tunneling spectra, and the conductance enhancement of the domelike feature is less than 1% (we also observed similar PC spectra observed with a Au tip; see Appendix D). The domelike feature was fitted considering chiral p-wave symmetry in Ref. [9]. Since there are other possibilities for fitting the ZBCP, e.g., conventional s-wave superconductor near T_c, here we just focus on gap value instead of fitting the spectra with specific models. Besides Ref. [9], other gap values have been measured, e.g., 1.1 mV from early Pt/SRO PC measurements [11,12], 0.38–0.5 mV from early STM measurements [13], 0.28 mV and 0.35 mV from recent STM measurements [14,41]. Here for W/SRO point contacts with different resistance and different pressure, and even in different locations and different runs, the 0.2 mV gap energy was observed consistently, and this gap value is comparable to that expected from $T_c = 1.5$ K from mean-field theory.

The broad background conductance dip in Fig. 1(a) for dI/dV at 625 Oe is generally called the zero-bias anomaly (ZBA), which is frequently observed in tunnel junctions [9] as well as PCs [12,42,43]. The possible origins for ZBA in PCs include "extrinsic" magnetic impurities, two-level systems, and Kondo scattering due to spontaneous electron spin polarization, as well as "intrinsic" density of states (DOS) effect. Early PC measurements show that the DOS of chromium is reduced due to the spin density wave gap [44], and recently for iron pnictides it has been shown that DOS is enhanced due to strong electron correlations [31,45]. Since SC in SRO is very sensitive to impurities, and here ZBA apparently coexists with SC, it is more likely due to "intrinsic" origin instead of impurities.

The background ZBA can be normalized when the bias dependence is replotted using $\ln(eV/k_BT)$. In Figs. 2(c) and 2(d), the normalized change of conductance shows a linear dependence for $eV \gg k_BT$, similar to what was observed in tunneling measurements for disordered metal films [46] and also for layered cuprates and manganites [47,48]. In the tunneling case, ZBA is attributed to the reduction of DOS due to electron-electron interaction (EEI), which can be also applied to PCS in the ballistic limit (see Appendix B for the justification of using tunneling theory for the ballistic portion of the PC resistance). As proposed by Altshuler and Aronov [49] for low-dimensional systems, EEI or more specifically the exchange interaction between electrons can cause quantum corrections to the conductivity and to the DOS, which depends on the dimensionality of the systems. For $eV \gg k_BT$, the DOS correction $\sim \ln(eV/k_BT)$ in 2D. When the thermal smearing is taken into account in the fitting and the full formula is used, we get good fits in the full bias range for the correction to conductance $\Delta G/G$ as shown by the dashed lines in Figs. 2(c) and 2(d) [also in Figs. 1(a) and 1(b)].

We note that in order for all $\Delta G/G$ curves to collapse onto the theoretical curve, an elevated temperature ($T_{\rm fit}$) needs to be assumed for data at lower temperatures; i.e., $eV/k_BT_{\rm fit}$ is used instead of $eV/k_BT_{\rm bulk}$, where $T_{\rm bulk}$ is the nominal temperature measured by the thermometer on the same silicon chip. This may indicate there is local heating in the small PC region, e.g., for PC in the thermal regime (see below and Appendix A for the model of PC resistance). Indeed at temperatures below 1 K, and particularly for mesoscopic samples, the electron temperature might be much higher than the bath temperature, in some cases due to inadequate filtering of the external microwave noise [50,51]. This elevated temperature may cause uncertainty to the fitting of ZBCP with p-wave symmetry, since even for s-wave SC, when T is close to T_c or the broadening parameter is large [52,53], the frequently observed double-peak spectra may smear into a domelike feature for a point contact junction with a finite barrier (see, e.g., Fig. 5 in Ref. [19]). To check whether such domelike feature evolves to a double-peak-like structure at lower temperatures, one needs to further cool down the PC, and an internal electron thermometer like $T_{\rm fit}$ from the EEI fitting is helpful.

The fitted curve can be considered as the normal state background and divided from the normalized conductance [9]; the resulting curves are shown in Figs. 2(e) and 2(f), with the domelike conductance enhancement well demonstrated. Another feature of the PC spectra in Figs. 2(e) and 2(f) is a small periodic "wiggling" outside ±0.2 mV, which also diminishes with increasing field and temperature. Since the resistivity along the c axis is about 1000 times larger than that in plane, the transport is presumably dominated by in-plane transport. The "wiggling" may be due to in-plane interference of quasiparticles for the S-S'-S junction configuration, where S' indicates the superconducting regime underneath the PC, as suggested by the decreasing period with increasing PC conductance/diameter. Similar "wiggling" was also observed for the multiple-band superconductor MgB_2 [17,19,54], and scattering of quasiparticles between bands could be another origin for the oscillation. For SRO, it was demonstrated [9] that multiple gap parameters could be involved in PC tunneling, which could be also related to the "wiggling."

C. Point contact resistance model and critical current dip

When the PC resistance is reduced from 9.3 Ω to 4.3 Ω, the ZBA background becomes less pronounced as shown in Figs. 3(c) and 3(d), while the conductance enhancement gets larger. This is better illustrated by the normalized enhancement [Fig. 4(d)], and by direct comparison of the zero field dI/dV [Fig. 4(c)]. To explain these changes, conventional the PC model (see Appendix A for details) can be introduced where the PC resistance is

$$R_{\rm PC} = R_{\rm Sh} + R_{\rm Max}, \tag{1}$$

where $R_{\rm Sh}$ is the Sharvin resistance corresponding to the ballistic limit, and $R_{\rm Max}$ is the Maxwell resistance corresponding to the diffusive limit which is related to the bulk resistivity ρ. For the simplest metallic PC with the 1D

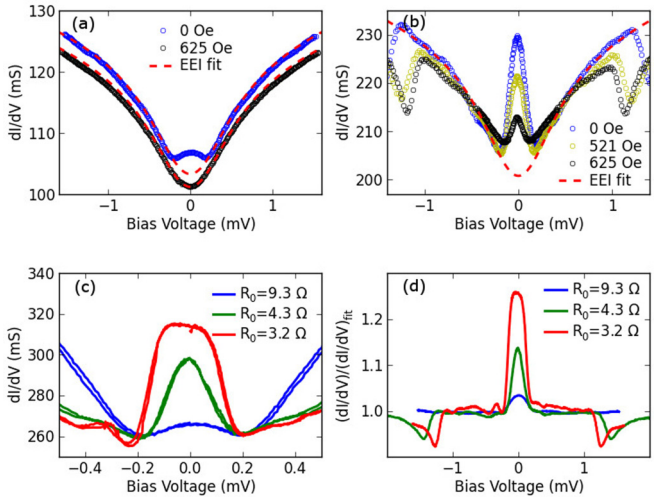

FIG. 4. (Color online) (a) dI/dV curves for the 9.3 Ω PC at 0 (blue), 625 Oe (black), and EEI fits (red dashed lines). (b) dI/dV curves for the 4.3 Ω PC at 0 (blue), 521 (yellow), 625 Oe (black), and the EEI fit for 0 Oe data. (c) Zoom-in of the zero-bias resistance dip regime with curves shifted for clarity except for the 3.2 Ω curve. The curves are reproducible for both ramping directions of the bias. (d) Zero-field conductance enhancement after being normalized with the fitted EEI background. All at 0.35 K.

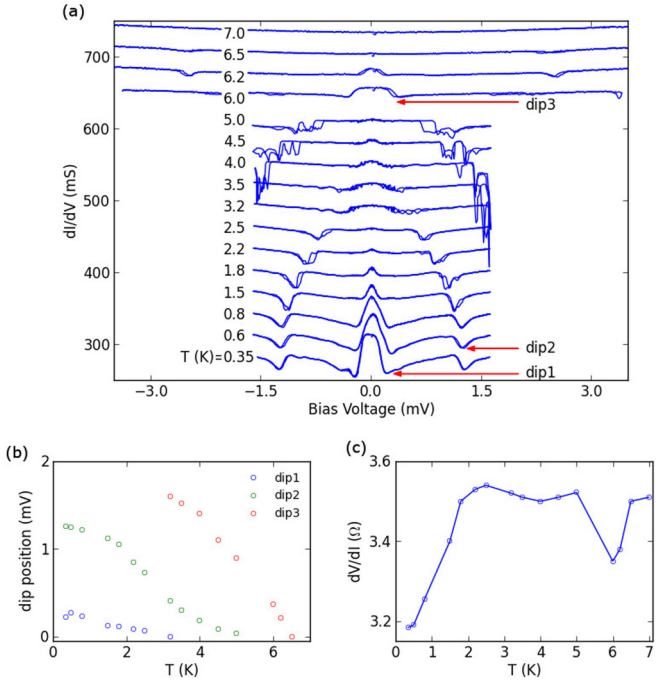

FIG. 5. (Color online) (a) For $R_0 = 3.2$ Ω three SC transitions are shown by dI/dV dips at different temperatures. (b) The position of the dI/dV dips vs temperature. (c) Zero-bias dV/dI vs temperature. Both (b) and (c) are derived from (a).

ballistic transport assumption, $R_{\rm Sh}$ is energy independent as the energy dependence of velocity cancels that of the DOS. But when SC, EEI, or complicated (3D) Fermi surfaces are involved [31,44,45], then the effective DOS may be probed by energy dependence of $R_{\rm Sh}$, i.e., the PC spectra. Here for single-crystal SRO the mean-free path is large, and when the diameter of the PC is smaller than the inelastic scattering length, the PC is close to the ballistic limit. Note that for the practical situation where multiple smaller PC junctions are formed in parallel within the contact footprint, the effective area of the PC is much smaller than that of the footprint [21,31]. In the conventional simple PC model $R_{\rm Sh} \propto (1/d)^2$ and $R_{\rm Max} \propto (\rho/d)$, where d is the diameter of PC, and ρ should be dominated by the in-plane resistivity for SRO. The reduction of resistance from 9.3 Ω to 4.3 Ω suggests an increase of d by roughly $\sqrt{9.3/4.3} = 1.47$ times in the ballistic limit (twice increase of the area), or by 2.2 times in the thermal limit(quadruple increase of the area).

With the increase of contact area, the PC may show a larger critical current (I_C) if the critical current density is constant and I_C is limited by the contact area. The additional dI/dV dips above 1 mV shown in Fig. 3 can be ascribed to the critical current effect [55,56], where I_C of the $R_{\rm Max}$ in series with $R_{\rm Sh}$ is reached. And indeed the dips are more pronounced when the ratio of $R_{\rm Max}/R_{\rm Sh}$ becomes larger when the total resistance $R_{\rm PC}$ gets smaller (see Appendix E for more measurement data). The $R_{\rm Max}$ is roughly 0.1 Ω as estimated by the resistance difference between the ZBA fit and the data curve above the dips. At 1.6 K the dip position is about 1.2 and 2.3 mV for the 4.3 Ω and 9.3 Ω PCs, respectively, so the calculated I_C is around 0.28 and 0.25 mA, respectively, inconsistent with the expected 2–4 times increase of I_C if it is proportional to the contact area $\sim d^2$. This finding suggests that I_C is determined by a fixed property, e.g., some SRO domain/surface regime under the PC, not just within the (effective) area of the PC itself. Thus, with increasing bias current, the $R_{\rm PC}$ shows a finite increase from $R_{\rm Sh}$ due to $R_{\rm Max}$, as described in Eq. (1) and demonstrated in Fig. 3.

When the PC resistance is further reduced to 3.2 Ω by pushing the tip to the SRO, even larger ZBCP is observed as shown in Fig. 1(e) and Fig. 4. After normalization by the background, the conductance enhancement at zero bias is about 3% for the 9.3 Ω PC, 14% for the 4.3 Ω PC, and 24% for the 3.2 Ω PC [Fig. 4(d)]. The original dI/dV curves without normalization for the 9.3 and 4.3 Ω PCs are shown in Figs. 4(a) and 4(b), and the EEI fits can very well reproduce the conductance correction with an effective temperature $T_{\rm fit}$. The EEI fit is no longer appropriate for lower $R_{\rm PC}$ when $R_{\rm Max}/R_{\rm Sh}$ becomes larger, since above the critical current dip the increase of $R_{\rm Max}$ leads to a clear conductance drop, as shown in Fig. 4(d). Zooming in on the zero-bias regime, the absolute amplitude of the ZBCP and of the "wiggling" are clearly shown in Fig. 4(c). We would like to emphasize again that for all three PCs in Fig. 4(c) the ZBCP evolves to ZBA background at around 0.2 mV, a gap value as expected from the weak-coupling theory.

The most striking feature is that the conductance dips persist to much higher temperatures than T_c of the bulk SRO, which is illustrated in Fig. 5. In Fig. 5(a), besides the first dI/dV dip at around 0.2 mV (this may not be a real dip but looks like one), there are two additional dI/dV dips; one persists up to about 5 K, while the other persists up to about 6.2 K. These two additional dI/dV dips are likely features related to SC, as the measured MR also shows hysteresis (see Appendix E for measurement data). The temperature dependence of the

position of dI/dV dips is plotted in Fig. 5(b), and the zero-bias dV/dI from the spectra in Fig. 5(a) is plotted in Fig. 5(c). There are clearly two resistance drops at around 4 and 6 K, and we note a similar but smaller resistance drop around 4 K was also observed in Ref. [9] for Au/SRO junctions. Since the bulk $T_c \leqslant 1.5$ K for sample S1, and even for the 3 K phase $T_c \sim 3$ K, here the greatly enhanced T_c should be only related to the W/SRO PC. Further investigation is required to clarify these probably new superconducting transitions.

IV. CONCLUSION

In summary, an ultralow-temperature point contact setup using nanopositioners was assembled and fresh contact interface can be made at liquid helium temperature to avoid surface reconstruction. Tungsten tips were used to penetrate the dead layer on the surface. Differential resistance of W/SRO point contact junctions is measured and we find (1) a domelike shape of zero-bias conductance enhancement within 0.2 mV, corresponding to a gap value comparable to that expected from mean-field theory; (2) a broad conductance dip background coexisting with superconductivity, which is ascribed to density of states effect due to 2D electron-electron interaction, and the retrieved electronic temperature may be useful for further analysis of the point contact spectra; (3) SC-like features persisting up to 6.2 K, much higher than the bulk T_c of SRO, presumably due to the pressure exerted by the W tip.

ACKNOWLEDGMENTS

We thank Hu Jin for contributions in the earlier stage of this project, Liang Liu for various helps with experiments and data analysis, Xin Lu and Yi-feng Yang for helpful discussions on point contact measurements, and Fa Wang for discussions on correlated systems. Work at Peking University is supported by the National Basic Research Program of China (973 Program) through Grants No. 2011CBA00106 and No. 2012CB927400. The work at Tulane is supported by the DOE under Grant No. DE-SC0012432.

APPENDIX A: MODEL OF POINT CONTACT RESISTANCE

There are many reviews on point contact spectroscopy [57], and particularly on unconventional heavy-fermion systems [58,59] and recently on anisotropic and multiband superconductors [19,60]. Here we first introduce the basics of the PC resistance following Ref. [58], then add pertinent discussions regarding our system.

In the simplified theoretical model, the PC is formed with an orifice with diameter d between two bulk metallic electrodes. Depending on the relative ratio between d and different mean-free path l, PCs can be categorized into three regimes: ballistic ($d < l_{\text{elastic}}$), diffusive ($l_{\text{elastic}} < d < l_{\text{inelastic}}$), and thermal ($d > l_{\text{inelastic}}$). In the ballistic regime, the Fermi surface in the two electrodes has a difference of eV, similar to the tunneling junction case, while in the thermal regime, the Fermi surface evolves smoothly within the PC and there is a well defined equilibrium temperature profile [61].

The current density in the orifice along its normal direction (z axis) is

$$j_z = 2e \sum_k (v_k)_z f_k(E), \tag{A1}$$

where v_k is the electron velocity, and $f_k(E)$ is the Fermi-Dirac distribution function. For a voltage-biased ballistic PC, considering the energy difference eV,

$$j_z = e \int_{E_F - eV/2}^{E_F + eV/2} dE \int \frac{d\Omega}{4\pi} v_z(E) f(E) N(E), \tag{A2}$$

where $N(E)$ is the electronic DOS. In the simplified 1D case (similar to planar tunneling), $v_z(E)$ is inversely proportional to $N(E)$; thus there is no nonlinearity caused by energy dependence of DOS. The resulting Ohmic resistance is

$$R_{\text{Sh}} = \frac{16 R_q}{(k_F d)^2} = \frac{16 \rho l}{3\pi d^2}, \tag{A3}$$

where ρ is the bulk resistivity, l the elastic mean-free path, $R_q = h/2e^2 = 12.9$ kΩ the quantum resistance. With the assumption that the Drude picture holds, $\rho l = p_F/ne^2$ is a constant for a particular metal, where Fermi momentum p_F and electronic density n were used in the original derivation. Thus, in the ballistic regime the diameter of the orifice d can be estimated using the zero-bias resistance R_0. To get a rough number, in the case of copper and other simple metals, $d \sim 30/\sqrt{R_0(\Omega)}$ nm.

At finite bias, the electron can also be backscattered by phonons, magnons, etc., at characteristic bias energy. So the I-V curve of the ballistic PC can be nonlinear and the second derivative is often used to identify phonon and magnon spectra. For correlated materials with a complex Fermi surface, $v_z(E)$ is no longer inversely proportional to $N(E)$, the I-V curve is nonlinear, and $R_{\text{Sh}}(E)$ may reflect the change of DOS [31,44,45]. More generally, other interactions such as the electron-electron interaction and superconductivity will also affect the DOS and be reflected in nonlinear I-V curves or point contact spectroscopy.

For PC in the diffusive or thermal regime, electrons in the PC are (inelastically) scattered by impurities or defects, whose contribution to R_{PC} can be estimated from the bulk resistivity, and the orifice just provides a geometric limitation for integration. In the limit $d \gg l_{\text{inelastic}}$, the Maxwell resistance is

$$R_{\text{Max}} = \frac{\rho}{d}. \tag{A4}$$

As it depends on d^{-1} instead of d^{-2}, it dominates over R_{Sh} when d is large. And when inelastic scattering happens inside the PC region, the equilibrium temperature in the PC can be elevated following

$$T_{\text{PC}}^2 = T_{\text{bath}}^2 + \frac{V^2}{4L}, \tag{A5}$$

where L is the Lorentz number. For a rough estimation, when $T_{\text{bath}} \ll T_{\text{PC}}$, assume a standard $L = 2.45 \times 10^{-8}$ V^2 K^{-2}, then $eV \sim 3.63 k_B T_{\text{PC}}$, or T_{PC} (K) $\simeq 3.2V$ (mV). This suggests that in the thermal limit, a similar feature can be found in the bias dependence of $dI/dV(V)$ and in the bath temperature

TABLE I. Summary of quasiparticle parameters of Sr_2RuO_4 (α,β,γ) [2] and tungsten.

Fermi sheet	α	β	γ	Tungsten
k_F (Å^{-1})	0.304	0.622	0.753	1.55
v_F (m s^{-1})	1.0×10^5	1.0×10^5	5.5×10^4	1.8×10^6
m^* (m_e)	3.3	7.0	16	1

dependence of $dI/dV(T)$. Here for SRO the gap energy is around 0.2 mV; in the thermal limit a rough estimation of T_{PC} at 0.2 mV is 0.64 K, which is still below T_C of SRO, so bias heating does not prevent observation of SC even in the thermal limit.

In the general situation, Wexler derived an interpolation formula [62],

$$R_{PC}(T) \simeq \frac{16\rho l}{3\pi d^2} + \frac{\rho(T)}{d}. \quad \text{(A6)}$$

For a heterocontact between two different electrodes (1 and 2), the resistance has contribution from both sides. For a geometrically symmetric PC with almost equal p_F,

$$R_{PC}(T) \simeq \frac{16\rho l}{3\pi d^2} + \frac{\rho_1(T) + \rho_2(T)}{2d}. \quad \text{(A7)}$$

Since the resistivity of a simple metal tip like tungsten is usually much smaller than that of the correlated electron systems (in the normal state), we may just keep the resistivity term of the correlated systems being probed. The assumption of equal p_F is very rough, the difference between $k_F = p_F/\hbar$ of tungsten and that of SRO is shown in Table I. Here k_F of tungsten is roughly estimated by assuming two valence electrons and a simple spherical Fermi surface.

In many cases it is found that although the footprint of the PC can be tens of microns, much larger than l, still a ballistic limit can be applied for fitting, which can be understood as that there are multiple smaller PC junctions randomly distributed across the contact region (the effective contact area is much smaller than the footprint) [21,63,64]. Although conceptually this is different from the picture that there is an interface barrier which contributes to the PC resistance like a planar tunneling junction, in both cases the ballistic limit can be applied when R_{Sh} is much larger than R_{Max}. More generally, one can add a finite R_{Max} in series or parallel as a fitting parameter.

For a heterocontact between a normal metal and a superconductor, the Blonder-Tinkham-Klapwijk (BTK) model [65] is widely used to explain the conductance enhancement within the gap energy. In the BTK model a tunnel barrier Z parameter is used to characterize the interface: for the clean interface, barrier parameter $Z = 0$; for the tunneling interface, barrier parameter $Z \geqslant 5$, and there is a continuous transition from metallic to tunneling limit. Whether the Fermi velocity mismatch can be fully represented with an effective Z parameter is not yet clear [59]. Note that in the BTK model inelastic scattering in the electrodes and the interface is not considered, even for finite Z, and thus $R_{Max} = 0$.

To take into account additional inelastic scattering at or near the interface, a finite R_{Max}, a normal resistor in series [56]. or a normal current in parallel [21,64] can be added to the tunneling term R_{Sh}. Thus even in the so-called thermal regime, it is possible to fit the PCS with the correct gap value with consideration of a combination of the BTK-dominated R_{Sh} and some extra inelastic term R_{Max}.

When the SC has unconventional pairing symmetries, the generalized BTK model is developed to fit the data by taking into account various parameters including order parameter symmetry, incidence angle, Fermi surface mismatch, lifetime broadening due to inter- or intraband scattering, etc. PCS for unconventional SC has been reviewed in Refs. [18,19,59,60]. It is still not clear whether the order parameter symmetry can be verified strictly from the shape of the point contact Andreev reflection spectra. In this work we mainly report the temperature and field dependence of the PC spectra rather than quantitatively fit the data with the generalized BTK model [9,10].

APPENDIX B: FITTING WITH THEORY OF ELECTRON-ELECTRON INTERACTION

As discussed in Appendix A, most normal metal–superconductor junction results can be well explained by the BTK model or generalized BTK models, where the tunneling barrier is characterized by the Z parameter; i.e., it can be thought as tunneling. In other words, the Sharvin resistance for ballistic transport can be understood as due to elastic tunneling of quantum tunneling channels with channel number equals $(k_F d)^{-2}$ [see Eq. (A3)].

More specifically, the slight difference between tunneling and planar tunneling (ballistic point contact is approaching this limit) is whether the in-plane momentum is conserved. While STM measures the integrated density of states, point contact (or planner tunneling) measures an effective density of states with consideration of in-plane momentum conservation [19,31]. This difference should be small for disordered films for which EEI is measured.

Correction to tunneling conductance by electron-electron interaction (EEI) due to reduction of density of states is quantitatively described by the Altshuler-Aronov (AA) theory [46,49]; in the 2D limit,

$$\frac{G(V,T) - G(0,T)}{G(0,T)} = \frac{e^2 R_{sq}}{8\pi^2\hbar} \ln\frac{4\pi\delta}{\mathcal{D}R_{sq}} \left[\Phi_2\left(\frac{eV}{k_B T}\right) - \Phi_2(0)\right], \quad \text{(B1)}$$

where R_{sq} is the resistance per square of the metal film, δ the thickness of the insulating barrier, $\mathcal{D}$ the diffusion constant, and Φ_2 is an integral for 2D as defined in Ref. [46]. The integral is

$$\Phi_d(A) = \int_{-\infty}^{\infty} dx \frac{\cosh(x + A) - 1}{\cosh(x/2)^2} \times \int_0^{\infty} dx \frac{\sinh y dy}{[\cosh y + \cosh(x + A)](1 + \cosh y) y^{2-d/2}}, \quad \text{(B2)}$$

where $x = \epsilon/kT$ and $A = eV/kT$.

The prefactor before the bracket in Eq. (B1) can be lumped into one parameter S and it is the only fitting parameter. When $eV \gg k_BT$ but still within the 2D limit, Eq. (B1) approaches $S \ln \frac{eV}{k_BT}$ and S is just the slope shown in Fig. 2. Since $R_{sq} = \rho/a$, a the thickness of the metal film, the resistivity $\rho = (e^2\nu\mathcal{D})^{-1}$, the slope $S \propto R_{sq} \ln(c\nu)$, where c is a constant.

For the 3D limit,

$$\frac{G(V,T) - G(0,T)}{G(0,T)} = \frac{e^2\rho}{8\sqrt{2}\pi^2\hbar}\left(\frac{k_BT}{\hbar\mathcal{D}}\right)^{1/2}\left[\Phi_3\left(\frac{eV}{k_BT}\right) - \Phi_3(0)\right], \quad \text{(B3)}$$

which shows a linear dependence on $\sqrt{eV/k_BT}$ when $eV \gg k_BT$.

In the main text Eq. (B1) is applied, and in Appendix D Eq. (B3) is used for PCs in other runs.

APPENDIX C: SAMPLE CHARACTERIZATION

Optical images for SRO crystal samples S1 and S2 are shown in Fig. 6 for comparison. Dense Ru inclusions of width about 1 μm and length a few μm are clearly seen in the microscope image for S2, which is also harder to cleave than S1. This is consistent to the observation of Lichtenberg in Ref. [66] that SRO with Ru vacancies is much easier to cleave and the surface dead layer probably is also easier to pierce through. We note that although here the surface was polished by sandpaper to improve image quality, the Ru inclusions can easily be observed on the surface of S2 without any treatment.

In separate runs, a conventional lock-in technique with room-temperature transformer coupling was used to measure the temperature dependence of resistance for bulk samples.

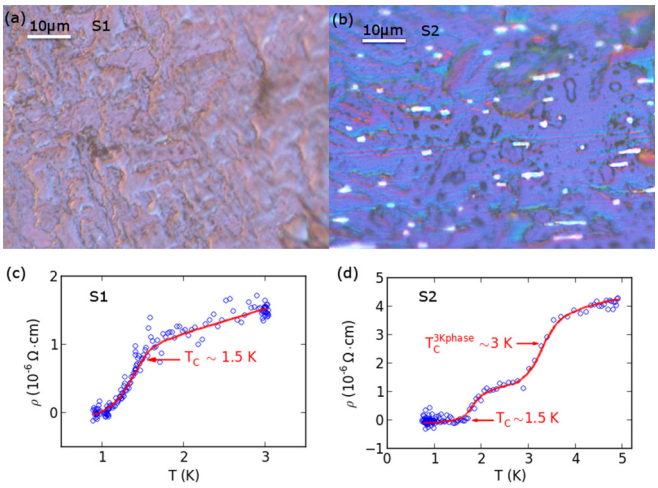

FIG. 6. (Color online) Comparison of polarized optical microscope images of sample S1 (a) and sample S2 (b). Ru inclusions are clearly seen in (b) for S2. Superconducting transition is shown for both samples by resistivity vs temperature measurement in (c) and (d). The red lines are guides to the eyes.

The lateral size of the samples is about 1 to 1.5 mm, the thickness about 0.5 mm, and the resistivity can be roughly estimated as shown in Fig. 6(c) and Fig. 6(d). Superconductivity of the SRO samples is verified and the transition temperature is around 1.5 K. We note that since the resistance is in the $\mu\Omega$ range large measurement current was applied which may cause some heating, so the temperature reading might not be accurate.

APPENDIX D: REPRODUCIBILITY

PC spectra for more than 10 locations were measured in several runs. In each run a few locations are tried to search for SC-like features. With increasing force the tip eventually became blunted and bent, and small cracks can also develop on the surface of the SRO. A set of PC spectra similar to that in the main text is shown in Fig. 7(a) for a W/SRO PC on S1 but obtained in another run. The gap value roughly around 0.15 mV is slightly smaller than 0.2 mV in the main text, possibly due to elevated local temperature, and the dips due to critical current effect at higher bias are again clearly shown.

Besides W tips, Au tips (0.5 mm diameter) were also tried on S1 and one of the PC spectra is shown in Fig. 7(b). For the Au/SRO PC, gap value around 0.5 mV is observed, the conductance enhancement is only about 1%, and instead of the domelike conductance peak, a split peak is observed, both similar to those features reported for in-plane Au/SRO tunneling junctions in Ref. [9].

In Fig. 7(b) ZBA is less obvious, although for some other Au/SRO PCs we have observed much clearer ZBA and also conductance dips. For W/SRO PCs, ZBA is more frequently observed, which could be due to a smaller contact area (the W tip does not deform like Au) and the thin barrier layer on the surface as observed in other PC measurements [64,67,68]. For those PC spectra showing clear ZBA, there are two typical types as shown in Fig. 8. One type is similar to that in Fig. 2 with a logarithmic dependence consistent with 2D EEI, and the SC feature sometimes coexists with ZBA; the other type has a $\sqrt{V}$ dependence which is consistent with 3D EEI; no clear SC feature is observed with this type of ZBA.

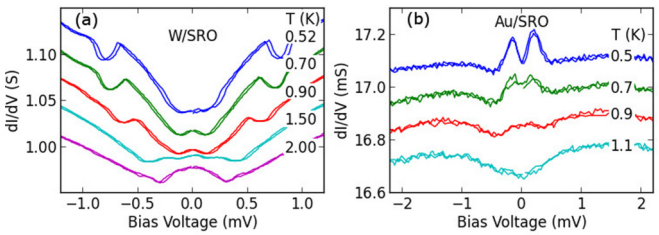

FIG. 7. (Color online) (a) Temperature dependence of the PC spectra for a W/SRO PC on S1 but obtained in another run, showing similar gap value and conductance dips as in the main text. The resistance is only about 1 Ω, so the heat dissipated around the PC should be larger. (b) Temperature dependence of the PC spectra for a Au/SRO PC on S1; a split peak within ±0.5 mV is observed, similar to that in Ref. [9].

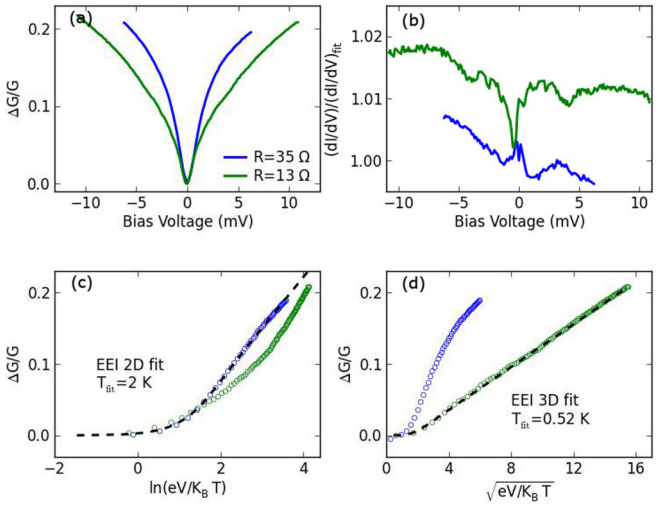

FIG. 8. (Color online) (a) Bias dependence of the normalized conductance for point contact on S2 with resistance 35 (blue) and 13 Ω (green) at $T = 0.52$ K, and (b) the conductance after being normalized by the background EEI fits (the green symbols are shifted up for clarity). (c) EEI 2D fitting (black dashed line) for the 13 Ω PC with $T_{\rm fit} = 2$ K, slope 0.07. (d) EEI 3D fitting for the 35 Ω PC with $T_{\rm fit} = 0.52$ K, slope (3D) = 0.015.

For the 2D EEI type, e.g., for a 35 Ω PC on S2 as shown in Fig. 8(c), the slope 0.07 is close to the slope 0.11 for S1 in Fig. 2, and 0.08 in Fig. 3, indicating a similar 2D EEI is probed, though here $T_{\rm fit} = 2$ K is higher than the bath temperature about 0.52 K, which is probably the reason why SC is not clearly observed. On the other hand, for another 13 Ω PC on S2 as shown in Fig. 8(d), the fitted temperature is close to the bath temperature. And it is possible Ru inclusion is probed.

In early works, ZBA or conductance dip background was also observed for Pt/SRO PCs [12], where with increasing field the ZBA becomes clearer and the origin is speculated to be related to some structural instabilities coupled to electronic and magnetic degrees of freedom. For in-plane Au/SRO tunneling junctions in Ref. [9], similar ZBA background was observed but only the normal-state ZBA was used to normalize the PC spectra so the superconducting spectra were stressed, as has been done frequently for PCS. It is worth noting that in Au/$Cu_xBi_2Se_3$ soft PCs, ZBA was also observed and ascribed to some pseudogap effect [68], while later in another work such V-shape conductance background is considered due to a nonideal surface layer [64]. Our work may help clarify this issue and provide a more specific interpretation for ZBA or conductance dip background in PCS.

APPENDIX E: ADDITIONAL MEASUREMENT DATA

For the 3.4 Ω point contact in the main text, magnetoresistance was also measured at two different temperatures as shown in Fig. 9(a). At 4 K, the hysteresis is still clear, and the total conductance change is close to that of the zero-bias

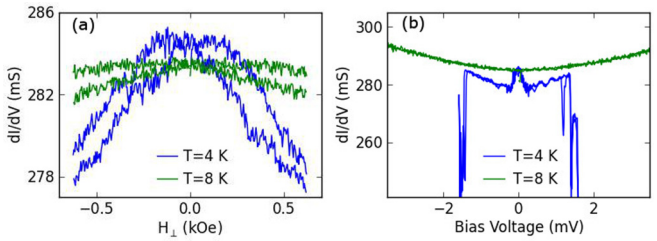

FIG. 9. (Color online) (a) Magnetoresistance at 4 K (blue) and 8 K (green) for the 3.4 Ω point contact. The hysteresis is clear at 4 K but not clear at 8 K since MR does not change much. (b) Bias dependence of the conductance for point contact at 4 K (blue) and 8 K (green) for the same contact, replotted with data in Fig. 5 for comparison with (a).

conductance enhancement due to SC as shown in Fig. 9(b). At 8 K, the hysteresis of MR is not clear, and the conductance decreases with increasing field, which is opposite to the trend in bias dependence of conductance. The above findings suggest that SC is still present at 4 K, but not at 8 K, and the MR hysteresis is closely related to SC.

To examine how much the critical current changes with point contact resistance, the normalized conductance for point contacts with different R_0 is shown in Fig. 10(a) at fixed temperature 1.8 K. We note that between the measurements in Fig. 10(a), the tip was pushed against the crystal and point contact resistance decreased; also field and temperature ramping were conducted as shown in the main text. The critical current can be roughly determined by the position of conductance dips [dip 2 in Fig. 5(a)], and is 0.29, 0.28, and 0.22 mA for 3.4, 4.3, and 9.3 Ω point contacts, respectively, which are surprisingly close to each other, which has been discussed in the main text.

After the 3.4 Ω PC, the resistance was increased to 19.5 Ω. In Fig. 10(b), the conductance dips for 9.3 Ω and 19.5 Ω point contacts are compared. The critical current for the 19.5 Ω PC is about 0.3 mA at 1.9 K, close to that of the 9.3 Ω PC at 1.8 K. The relative size of the conductance dip becomes smaller for larger contact resistance, which can be understood since for larger $R_{\rm Sh}$, the ratio of $R_{\rm Max}/(R_{\rm Max} + R_{\rm Sh})$ is smaller [55,56].

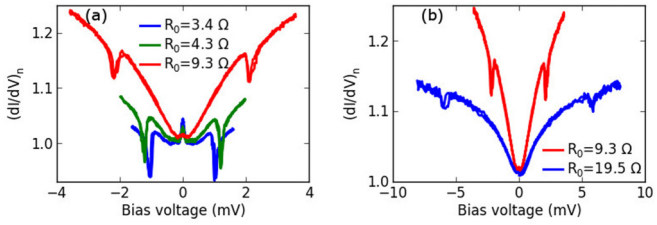

FIG. 10. (Color online) (a) Bias dependence of the normalized conductance for point contacts with different R_0 at the same location, all at 1.8 K. The contact resistance decreases with increasing pressure. The critical current dips appear at bias voltage proportional to R_0. (b) At $T = 1.9$ K, the position of the critical current dips for the 19.5 Ω PC is still proportional to R_0. The 9.3 Ω data from (a) are replotted here for comparison.

[1] Y. Maeno, H. Hashimoto, K. Yoshida, S. Nishizaki, T. Fujita, J. G. Bednorz, and F. Lichtenberg, Superconductivity in a layered perovskite without copper, Nature (London) **372**, 532 (1994).

[2] A. P. Mackenzie and Y. Maeno, The superconductivity of Sr_2RuO_4 and the physics of spin-triplet pairing, Rev. Mod. Phys. **75**, 657 (2003).

[3] Y. Maeno, S. Kittaka, T. Nomura, S. Yonezawa, and K. Ishida, Evaluation of spin-triplet superconductivity in Sr_2RuO_4, J. Phys. Soc. Jpn. **81**, 011009 (2012).

[4] G. M. Luke, Y. Fudamoto, K. M. Kojima, M. I. Larkin, J. Merrin, B. Nachumi, Y. J. Uemura, Y. Maeno, Z. Q. Mao, Y. Mori, H. Nakamura, and M. Sigrist, Time-reversal symmetry-breaking superconductivity in Sr_2RuO_4, Nature (London) **394**, 558 (1998).

[5] J. Xia, Y. Maeno, P. T. Beyersdorf, M. M. Fejer, and A. Kapitulnik, High resolution polar kerr effect measurements of Sr_2RuO_4: Evidence for broken time-reversal symmetry in the superconducting state, Phys. Rev. Lett. **97**, 167002 (2006).

[6] J. R. Kirtley, C. Kallin, C. W. Hicks, E.-A. Kim, Y. Liu, K. A. Moler, Y. Maeno, and K. D. Nelson, Upper limit on spontaneous supercurrents in Sr_2RuO_4, Phys. Rev. B **76**, 014526 (2007).

[7] C. W. Hicks, J. R. Kirtley, T. M. Lippman, N. C. Koshnick, M. E. Huber, Y. Maeno, W. M. Yuhasz, M. B. Maple, and K. A. Moler, Limits on superconductivity-related magnetization in Sr_2RuO_4 and $PrOs_4Sb_{12}$ from scanning squid microscopy, Phys. Rev. B **81**, 214501 (2010).

[8] P. J. Curran, S. J. Bending, W. M. Desoky, A. S. Gibbs, S. L. Lee, and A. P. Mackenzie, Search for spontaneous edge currents and vortex imaging in Sr_2RuO_4 mesostructures, Phys. Rev. B **89**, 144504 (2014).

[9] S. Kashiwaya, H. Kashiwaya, H. Kambara, T. Furuta, H. Yaguchi, Y. Tanaka, and Y. Maeno, Edge states of Sr_2RuO_4 detected by in-plane tunneling spectroscopy, Phys. Rev. Lett. **107**, 077003 (2011).

[10] S. Kashiwaya, H. Kashiwaya, K. Saitoh, Y. Mawatari, and Y. Tanaka, Tunneling spectroscopy of topological superconductors, Phys. E (Amsterdam, Neth.) **55**, 25 (2014).

[11] F. Laube, G. Goll, H. v. Löhneysen, M. Fogelström, and F. Lichtenberg, Spin-triplet superconductivity in Sr_2RuO_4 probed by Andreev reflection, Phys. Rev. Lett. **84**, 1595 (2000).

[12] G. Goll, Andreev-reflection experiments on layered superconductors, Phys. B (Amsterdam, Neth.) **383**, 71 (2006).

[13] M. D. Upward, L. P. Kouwenhoven, A. F. Morpurgo, N. Kikugawa, Z. Q. Mao, and Y. Maeno, Direct observation of the superconducting gap of Sr_2RuO_4, Phys. Rev. B **65**, 220512 (2002).

[14] I. A. Firmo, S. Lederer, C. Lupien, A. P. Mackenzie, J. C. Davis, and S. A. Kivelson, Evidence from tunneling spectroscopy for a quasi-one-dimensional origin of superconductivity in Sr_2RuO_4, Phys. Rev. B **88**, 134521 (2013).

[15] R. Matzdorf, Z. Fang, Ismail, J. Zhang, T. Kimura, Y. Tokura, K. Terakura, and E. W. Plummer, Ferromagnetism stabilized by lattice distortion at the surface of the p-wave superconductor Sr_2RuO_4, Science **289**, 746 (2000).

[16] S. Lederer, W. Huang, E. Taylor, S. Raghu, and C. Kallin, Suppression of spontaneous currents in Sr_2RuO_4 by surface disorder, Phys. Rev. B **90**, 134521 (2014).

[17] R. S. Gonnelli, A. Calzolari, D. Daghero, G. A. Ummarino, V. A. Stepanov, P. Fino, G. Giunchi, S. Ceresara, and G. Ripamonti, Temperature and junction-type dependency of Andreev reflection in MgB_2, J. Phys. Chem. Solids **63**, 2319 (2002).

[18] K. Gloos, F. Anders, B. Buschinger, C. Geibel, K. Heuser, F. Jährling, J. S. Kim, R. Klemens, R. Müller-Reisener, C. Schank, and G. Stewart, Scaling behavior of point contacts between a tungsten tip and the heavy-fermion superconductors, J. Low Temp. Phys. **105**, 37 (1996).

[19] D. Daghero and R. S. Gonnelli, Probing multiband superconductivity by point-contact spectroscopy, Supercond. Sci. Technol. **23**, 043001 (2010).

[20] K. Gloos, F. Martin, C. Schank, C. Geibel, and F. Steglich, Pressure effects in point contacts with heavy-fermion $CeCu_2Ge_2$, Phys. B (Amsterdam, Neth.) **206-207**, 279 (1995).

[21] Y. Miyoshi, Y. Bugoslavsky, and L. F. Cohen, Andreev reflection spectroscopy of niobium point contacts in a magnetic field, Phys. Rev. B **72**, 012502 (2005).

[22] S. Kittaka, H. Taniguchi, S. Yonezawa, H. Yaguchi, and Y. Maeno, Higher-Tc superconducting phase in Sr_2RuO_4 induced by uniaxial pressure, Phys. Rev. B **81**, 180510 (2010).

[23] S. Kittaka, H. Yaguchi, and Y. Maeno, Large enhancement of 3-k phase superconductivity in the Sr_2RuO_4-Ru eutectic system by uniaxial pressure, J. Phys. Soc. Jpn. **78**, 103705 (2009).

[24] C. W. Hicks, D. O. Brodsky, E. A. Yelland, A. S. Gibbs, J. A. N. Bruin, M. E. Barber, S. D. Edkins, K. Nishimura, S. Yonezawa, Y. Maeno, and A. P. Mackenzie, Strong increase of Tc of Sr_2RuO_4 under both tensile and compressive strain, Science **344**, 283 (2014).

[25] Z. Q. Mao, Y. Maenoab, and H. Fukazawa, Crystal growth of Sr_2RuO_4, Mater. Res. Bull. **35**, 1813 (2000).

[26] H. Taniguchi, S. Kittaka, S. Yonezawa, H. Yaguchi, and Y. Maeno, Field-temperature phase diagram of superconductivity in Sr_2RuO_4-Ru under out-of-plane uniaxial pressure, J. Phys.: Conf. Ser. **391**, 012108 (2012).

[27] Y. A. Ying, Y. Xin, B. W. Clouser, E. Hao, N. E. Staley, R. J. Myers, L. F. Allard, D. Fobes, T. Liu, Z. Q. Mao, and Y. Liu, Suppression of proximity effect and the enhancement of p-wave superconductivity in the Sr_2RuO_4-Ru system, Phys. Rev. Lett. **103**, 247004 (2009).

[28] Y. A. Ying, N. E. Staley, Y. Xin, K. Sun, X. Cai, D. Fobes, T. J. Liu, Z. Q. Mao, and Y. Liu, Enhanced spin-triplet superconductivity near dislocations in Sr_2RuO_4, Nat. Commun. **4**, 2596 (2013).

[29] D. A. Dikin, M. Mehta, C. W. Bark, C. M. Folkman, C. B. Eom, and V. Chandrasekhar, Coexistence of superconductivity and ferromagnetism in two dimensions, Phys. Rev. Lett. **107**, 056802 (2011).

[30] K. Deguchi, Z. Q. Mao, and Y. Maeno, Determination of the superconducting gap structure in all bands of the spin-triplet superconductor Sr_2RuO_4, J. Phys. Soc. Jpn. **73**, 1313 (2004).

[31] W.-C. Lee, W. K. Park, H. Z. Arham, L. H. Greene, and P. Phillips, Theory of point contact spectroscopy in correlated materials, Proc. Natl. Acad. Sci. U.S.A. **112**, 651 (2015).

[32] I. Lukyanchuk, V. M. Vinokur, A. Rydh, R. Xie, M. V. Milošević, U. Welp, M. Zach, Z. L. Xiao, G. W. Crabtree, S. J. Bending, F. M. Peeters, and W. K. Kwok, Rayleigh instability of confined vortex droplets in critical superconductors, Nat. Phys. **11**, 21 (2015).

[33] E. Dumont and A. C. Mota, Unconventional vortex dynamics in superconducting states with broken time-reversal symmetry, Phys. Rev. B **65**, 144519 (2002).

[34] H. Kambara, S. Kashiwaya, H. Yaguchi, Y. Asano, Y. Tanaka, and Y. Maeno, Anomalous transport through the *p*-wave superconducting channel in the 3-K phase of Sr_2RuO_4, Phys. Rev. Lett. **101**, 267003 (2008).

[35] A. Palau, H. Parvaneh, N. A. Stelmashenko, H. Wang, J. L. Macmanus-Driscoll, and M. G. Blamire, Hysteretic vortex pinning in superconductor-ferromagnet nanocomposites, Phys. Rev. Lett. **98**, 117003 (2007).

[36] S.-I. Ikeda, Y. Maeno, S. Nakatsuji, M. Kosaka, and Y. Uwatoko, Ground state in $Sr_3Ru_2O_7$: Fermi liquid close to a ferromagnetic instability, Phys. Rev. B **62**, R6089 (2000).

[37] S. I. Ikeda, S. Koiwai, Y. Yoshida, N. Shirakawa, S. Hara, M. Kosaka, and Y. Uwatoko, Magnetization of single crystalline strontium ruthenate under uniaxial-pressure, J. Magn. Magn. Mater. **272**, E293 (2004).

[38] J. P. Carlo, T. Goko, I. M. Gat-Malureanu, P. L. Russo, A. T. Savici, A. A. Aczel, G. J. MacDougall, J. A. Rodriguez, T. J. Williams, G. M. Luke, C. R. Wiebe, Y. Yoshida, S. Nakatsuji, Y. Maeno, T. Taniguchi, and Y. J. Uemura, New magnetic phase diagram of $(Sr,Ca)_2RuO_4$, Nat. Mater. **11**, 323 (2012).

[39] J. E. Ortmann, J. Y. Liu, J. Hu, M. Zhu, J. Peng, M. Matsuda, X. Ke, and Z. Q. Mao, Competition between antiferromagnetism and ferromagnetism in Sr_2RuO_4 Probed by Mn and Co doping, Sci. Rep. **3**, 2950 (2013).

[40] I. K. Yanson, O. P. Balkashin, V. V. Fisun, Y. I. Yanson, and Y. G. Naidyuk, Current-field diagram for the magnetic states of a surface spin valve in a point contact with a single ferromagnetic film, Low Temp. Phys. **39**, 279 (2013).

[41] H. Suderow, V. Crespo, I. Guillamon, S. Vieira, F. Servant, P. Lejay, J. P. Brison, and J. Flouquet, A nodeless superconducting gap in Sr_2RuO_4 from tunneling spectroscopy, New J. Phys. **11**, 093004 (2009).

[42] K. Gloos, An alternative view at the zero-bias anomaly of metallic point contacts, Low Temp. Phys. **35**, 935 (2009).

[43] K. Gloos and E. Tuuli, Break-junction experiments on the zero-bias anomaly of non-magnetic and ferromagnetically ordered metals, J. Phys.: Conf. Ser. **400**, 042011 (2012).

[44] H. Meekes, Point-contact spectroscopy in incommensurate chromium, Phys. Rev. B **38**, 5924 (1988).

[45] H. Z. Arham, C. R. Hunt, W. K. Park, J. Gillett, S. D. Das, S. E. Sebastian, Z. J. Xu, J. S. Wen, Z. W. Lin, Q. Li, G. Gu, A. Thaler, S. Ran, S. L. Bud'ko, P. C. Canfield, D. Y. Chung, M. G. Kanatzidis, and L. H. Greene, Detection of orbital fluctuations above the structural transition temperature in the iron pnictides and chalcogenides, Phys. Rev. B **85**, 214515 (2012).

[46] M. E. Gershenzon, V. N. Gubankov, and M. I. Faleĭ, Zh. Eksp. Teor. Fiz. **90**, 2196 (1986) [Tunnel spectroscopy of the electron-electron interaction in disordered aluminum films, Sov. Phys. JETP **63**, 1287 (1986)].

[47] A. A. Abrikosov, Quantum interference effects in quasi-two-dimensional metals, Phys. Rev. B **61**, 7770 (2000).

[48] D. Mazur, K. E. Gray, J. F. Zasadzinski, L. Ozyuzer, I. S. Beloborodov, H. Zheng, and J. F. Mitchell, Redistribution of the density of states due to coulomb interactions in lsmo, Phys. Rev. B **76**, 193102 (2007).

[49] B. L. Altshuler and A. G. Aronov, Zh. Eksp. Teor. Fiz. **77**, 2028 (1979) [Contribution to the theory of disordered metals in strongly doped semiconductors, Sov. Phys. JETP **50**, 968 (1979)]; B. L. Altshuler, A. G. Aronov, and P. A. Lee, Interaction effects in disordered fermi systems in two dimensions, Phys. Rev. Lett. **44**, 1288 (1980); B. L. Altshuler and A. G. Aronov, in *Electron-Electron Interactions in Disordered Systems*, Modern Problems in Condensed Matter Sciences, Vol. 10, edited by M. Pollak and A. L. Efros (North-Holland, Amsterdam, 1985), Chap. 1, pp. 1–154.

[50] L. Liu, J. Niu, L. Xiang, J. Wei, D.-L. Li, J.-F. Feng, X.-F. Han, X.-G. Zhang, and J. M. D. Coey, Symmetry-dependent electron-electron interaction in coherent tunnel junctions resolved by measurements of zero-bias anomaly, Phys. Rev. B **90**, 195132 (2014).

[51] J. Wei, S. Pereverzev, and M. E. Gershenson, Microwave-induced dephasing in one-dimensional metal wires, Phys. Rev. Lett. **96**, 086801 (2006).

[52] Y. Bugoslavsky, Y. Miyoshi, S. K. Clowes, W. R. Branford, M. Lake, I. Brown, A. D. Caplin, and L. F. Cohen, Possibilities and limitations of point-contact spectroscopy for measurements of spin polarization, Phys. Rev. B **71**, 104523 (2005).

[53] J. Wei, G. Sheet, and V. Chandrasekhar, Possible microscopic origin of large broadening parameter in point Andreev reflection spectroscopy, Appl. Phys. Lett. **97**, 062507 (2010).

[54] Y. Bugoslavsky, Y. Miyoshi, G. K. Perkins, A. D. Caplin, L. F. Cohen, A. V. Pogrebnyakov, and X. X. Xi, Effect of magnetic field on the two superconducting gaps in MgB_2, Phys. Rev. B **69**, 132508 (2004).

[55] L. Shan, H. J. Tao, H. Gao, Z. Z. Li, Z. A. Ren, G. C. Che, and H. H. Wen, *s*-wave pairing in $MgCNi_3$ revealed by point contact tunneling, Phys. Rev. B **68**, 144510 (2003).

[56] G. Sheet, S. Mukhopadhyay, and P. Raychaudhuri, Role of critical current on the point-contact Andreev reflection spectra between a normal metal and a superconductor, Phys. Rev. B **69**, 134507 (2004).

[57] A. M. Duif, A. G. M. Jansen, and P. Wyder, Point-contact spectroscopy, J. Phys.: Condens. Matter **1**, 3157 (1989).

[58] Y. G. Naidyuk and I. K. Yanson, Point-contact spectroscopy of heavy-fermion systems, J. Phys.: Condens. Matter **10**, 8905 (1998).

[59] W. K. Park and L. H. Greene, Andreev reflection and order parameter symmetry in heavy-fermion superconductors: The case of $CeCoIn_5$, J. Phys.: Condens. Matter **21**, 103203 (2009).

[60] D. Daghero, M. Tortello, P. Pecchio, V. A. Stepanov, and R. S. Gonnelli, Point-contact Andreev-reflection spectroscopy in anisotropic superconductors: The importance of directionality (review article), Low Temp. Phys. **39**, 199 (2013).

[61] H. Pothier, S. Gueron, N. O. Birge, D. Esteve, and M. H. Devoret, Energy distribution function of quasiparticles in mesoscopic wires, Phys. Rev. Lett. **79**, 3490 (1997).

[62] G. Wexler, The size effect and the non-local boltzmann transport equation in orifice and disk geometry, Proc. Phys. Soc., London **89**, 927 (1966).

[63] Y. Bugoslavsky, Y. Miyoshi, G. K. Perkins, A. D. Caplin, L. F. Cohen, A. V. Pogrebnyakov, and X. X. Xi, Electron diffusivities in MgB_2 from point contact spectroscopy, Phys. Rev. B **72**, 224506 (2005).

[64] H. Peng, D. De, B. Lv, F. Wei, and C.-W. Chu, Absence of zero-energy surface bound states in $Cu_xBi_2Se_3$ studied via Andreev reflection spectroscopy, Phys. Rev. B **88**, 024515 (2013).

[65] G. E. Blonder, M. Tinkham, and T. M. Klapwijk, Transition from metallic to tunneling regimes in superconducting microconstrictions: Excess current, charge imbalance, and supercurrent conversion, Phys. Rev. B **25**, 4515 (1982).

[66] F. Lichtenberg, The story of Sr_2RuO_4, Prog. Solid State Chem. **30**, 103 (2002).

[67] L. Shan, Y. Huang, H. Gao, Y. Wang, S. L. Li, P. C. Dai, F. Zhou, J. W. Xiong, W. X. Ti, and H. H. Wen, Distinct pairing symmetries in $Nd_{1.85}Ce_{0.15}CuO_{4-y}$ and $La_{1.89}Sr_{0.11}CuO_4$ single crystals: Evidence from comparative tunneling measurements, Phys. Rev. B **72**, 144506 (2005).

[68] S. Sasaki, M. Kriener, K. Segawa, K. Yada, Y. Tanaka, M. Sato, and Y. Ando, Topological superconductivity in $Cu_xBi_2Se_3$, Phys. Rev. Lett. **107**, 217001 (2011).